Original article: Solar Energy Materials & Solar Cells 246 (2022) 111909
Original DOI: https://doi.org/10.1016/j.solmat.2022.111909
This version is revised in accordance with the Corrigendum published as https://doi.org/10.1016/j.solmat.2023.112254

Inaccuracies in Contact Resistivity from the Cox-Strack Method: a Review

Bas van Wijngaarden, Junchun Yang, Jurriaan Schmitz*

[a]*University of Twente, P.O. Box 217, 7500 AE Enschede, Netherlands*

Abstract

Recently, the Cox-Strack method for contact resistivity determination is increasingly used in the context of photovoltaic cell engineering. This document reviews the literature published in the period 2017-2021 containing Cox-Strack measurement results. As the Cox-Strack method is error-prone, we analyze this literature on the possible inaccuracies that may arise due to (1) approximations by Cox and Strack, (2) the choice of contact diameters, and (3) resistive coatings. On the basis of our findings, more than half of the 93 reviewed articles may need additional analysis for an accurate quantification of the lower reported contact resistance values. The article concludes with recommendations for an improved Cox-Strack methodology.

Keywords: Electrical characterization, solar cells, contact resistivity, measurement errors, metal-semiconductor junctions, test structures, photovoltaics

1. Introduction

In the pursuit of high-efficiency solar cells, novel contact architectures play a prominent role. After improvements of bulk silicon carrier lifetimes, the metal-semiconductor contacts in mass-produced silicon cells have become the main bottleneck for further efficiency gains [1]. Such contacts exhibit contact resistivity and surface recombination, both leading to efficiency losses [2]. The surface recombination is easiest countered by using smaller-area contacts; this however immediately raises the bar for contact resistivity reduction efforts. For resistive losses to become negligible in conventional silicon solar cells, the contact resistivity of a fully covered (backside) contact should be below 100 mΩcm^2. For line-shaped contacts with 5% surface coverage, the target is to get below 2 mΩcm^2 [3].

Recent scientific literature shows a fast rise in the number of articles investigating metal-semiconductor contact technology, in pursuit of carrier-selective contacts and bifacial cell architectures. A common method to quantify the contact resistivity is the Cox-Strack method published in [4]. In the photovoltaics literature, this article is commonly cited since 2017 as illustrated by Figure 1. The popularity of the Cox-Strack method stems from its simplicity and the compatibility with solar cell manufacturing (except that no p-n junction should be present).

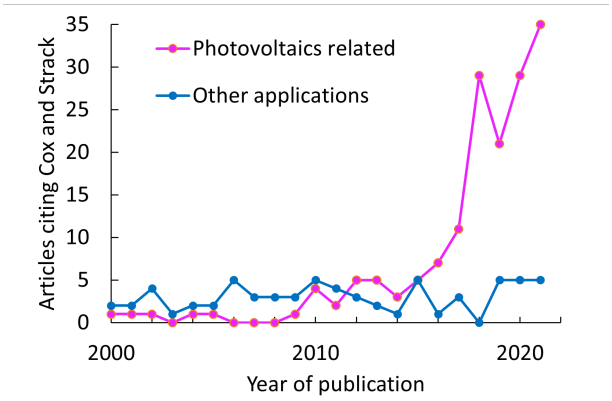

Figure 1: Overview of documents citing the original Cox-Strack paper in the Scopus database [5], showing a steep increase of photovoltaics-related articles since 2017. (The other articles mostly deal with contacts to high-bandgap semiconductors or thermoelectric materials.)

This contact resistivity measurement method however has issues with accuracy, as reported by several authors (e.g. [6–9]). This review studies the accuracy of resistivity values published in the years 2017-2021 in the photovoltaics literature. It starts with a description of the Cox-Strack method and its limitations in Section 2 and a documentation of the followed approach (Section 3). Then, we treat the accuracy of recently published contact resistivity values in Sections 4–6. The findings are then discussed and used to formulate recommendations for application of this measurement

*Corresponding author. E-mail: j.schmitz@utwente.nl

method.

2. The Cox-Strack Method

The Cox-Strack method is based on the assumption that the total resistance R_T measured between two terminals on opposite sides of a semiconductor can be expressed as:

$$R_T = R_c + R_s + R_0 \tag{1}$$

where R_c is the contact resistance of a (small-area) top contact on the semiconductor, R_s is the spreading resistance in the semiconducting substrate, and R_0 the (small) residual resistance of a large-area backside contact, as depicted in Fig. 2. Although equation 1 is a simplification [9], it generally holds sufficiently well for this three-layer stack.

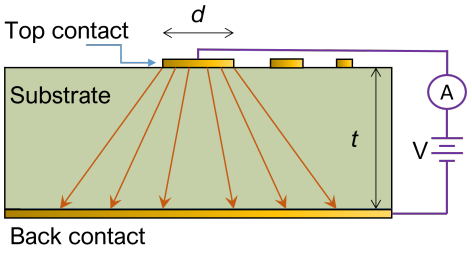

Figure 2: Configuration of the conventional Cox-Strack measurement. The total resistance R_T is measured from a top contact with diameter d through a semiconducting substrate with thickess t to a back contact, by application of a dc voltage V and measurement of the current.

Cox and Strack proceed to express R_c in terms of contact resistivity ρ_c, assuming uniform current flow and an isotropic contact, as:

$$R_c = \frac{\rho_c}{\frac{1}{4}\pi d^2} \tag{2}$$

where d is the diameter of the top contact.

The spreading resistance R_s in the semiconductor depends on its geometry and resistivity in a non-trivial manner. By lack of finite element simulation tools, Cox and Strack used an electrolytic tank setup to estimate this dependency, and proposed the approximate relationship:

$$R_s \approx \frac{\rho_w}{\pi d} \arctan\left(\frac{4t}{d}\right) \tag{3}$$

with ρ_w the wafer resistivity and t the semiconductor thickness.

The final term in equation 1, R_0, is presumed constant and rather low. When the total resistance of a series of contacts with different diameters is measured, the contact resistivity can then be found from the slope of a linear fit to R_T - R_s versus $1/d^2$. (The dimensions and wafer resistivity are assumed known to sufficient precision.) This procedure, employing equations 1,2,3 is the conventional Cox-Strack method.

Later works (e.g. [6, 7, 9]) proved particularly equation 3 inaccurate, leading to a significant overestimate of the contact resistivity. This systematic error $\Delta\rho_c$ was estimated to amount to [9]:

$$\frac{\Delta\rho_c}{\rho_c} \approx 1.2\% \frac{\rho_w t}{\rho_c} \tag{4}$$

An exact solution for the spreading resistance as published by Gelmont and Shur [10] finds little use, probably because of its complicated form. More straightforward, approximating equations have been proposed that better fit to finite element simulations [6, 9, 11]. In this article we use the approximation from [9]:

$$R_s \approx \frac{2\rho_w}{\pi d}\left[\frac{d}{2t} + \frac{4}{\pi} + \left(1 - \frac{4}{\pi}\right)\arctan\left(\frac{2d}{3t}\right)\right]^{-1}. \tag{5}$$

Besides the issue with equation 3, the Cox-Strack method is inherently inaccurate when only large diameters are used, because for large d the spreading resistance is proportional to $1/d^2$, just like the contact resistance, making them indistinguishable. One requires diameters $d < 2t$ to quantify the contact resistivity with good accuracy [9]. Further, it is obviously necessary, in view of equation 1, that R_c should be significant with respect to R_s for a measurement to quantify the former.

Several modifications to the conventional Cox-Strack method have been proposed in literature. In case of non-ohmic, Schottky-type contacts, resistance can be determined by the method of Cheung and Cheung [12]; see also [13]. Several papers in this review make use of that extension for metal oxide based contacts to silicon.

3. Approach

In our investigation, we started off with all documents published in the period 2017-2021 that cite [4] according to the Scopus literature database [5]. Articles were only considered for this study if they:

- report resistivity results determined with the Cox-Strack method;
- relate to photovoltaics;
- are non-retracted journal or conference papers;
- use contacts that can be assumed laterally uniform.

Table 1 summarizes the number of articles in Scopus and the outcome of this selection procedure. The first criterion above leads to 'no data' rejects, while the other three yield 'other' rejected articles.

Table 1: Articles considered for this work. Some articles present no (new) resistivity data using the Cox-Strack method or are discarded for other reasons (see main text).

Year	Scopus	No data	Other	Used in this study
2017	14	5	3	6 [14–19]
2018	29	4	4	21 [8, 20–39]
2019	26	9	2	15 [40–54]
2020	34	14	0	20 [55–74]
2021	40	8	1	31 [11, 75–104]
Total	142	39	10	93

For this review, we retrieved the values of several parameters of relevance for the Cox-Strack method from the selected articles (if reported). These are the wafer resistivity, wafer thickness, contact diameters and contact resistivities. Further, if a multilayer top contact is investigated (see Section 6), we also recorded the sheet resistance and layer thickness of the employed conductive coating.

Wafer resistivities are often reported as a range, e.g. 1-5 Ωcm. In this case we assumed the central value. Graphically represented data were quantified using GraphGrabber [105]. Corresponding authors were approached in case the necessary information could not be found in the article or its supporting information. Of the 57 contacted corresponding authors, we obtained 28 replies.

4. Inaccuracies from the Cox-Strack equation

The conventional Cox-Strack method becomes inaccurate when the contact resistivity is low compared to the product of wafer resistivity and wafer thickness, $\rho_w t$ [9]. This affects the lowest reported contact resistivity values most. Figure 3 presents these values for all selected articles, along with the $\rho_w t$ product.

Diagonal dashed lines in the figure indicate thresholds of systematic inaccuracy according to equation 4. As evident from the figure, some of the lowest reported ρ_c values in recent literature may be significantly off: 13% of the investigated articles report values that are more than 10% overestimated. The systematic error in those works could be reduced with a factor 4 [9] by using a more accurate spreading resistance equation than eq. 3. As the error is systematic and approximated by

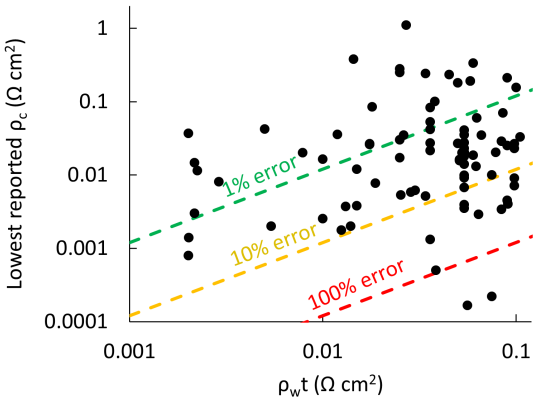

Figure 3: The lowest reported contact resistivity in each of the studied papers, as a function of the product of wafer resistivity ρ_w and wafer thickness t if provided (90 articles). Dashed lines indicate a systematic error of 1% (green), 10% (orange) and 100% (red) introduced by the use of equation 3.

eq. 4, the determined contact resistivity ρ_c can also be corrected for this effect as:

$$\rho_c^{corr} = \rho_c - 1.2\%\rho_w t. \quad (6)$$

5. The choice of contact diameters

5.1. The smallest top contact

The Cox-Strack approach requires the total resistance measurement on several circular top contacts with varying diameter d. The minimum number of contacts to be measured is given by the number of degrees of freedom (unknown parameter values) in the Cox-Strack equation, normally 2 or 3: ρ_c, ρ_w and R_0. It is common practice to probe more than this minimum number, typically 4-10 contacts.

However, only a careful choice of diameters leads to an accurate extraction of ρ_c. Figure 4 illustrates this for typical dimensions and materials in solar cell research. The theoretical curves come very close together for contact resistivities below 10 mΩcm^2. To distinguish them requires precise measurements and contacts with low d. Moreover, for the chosen dimensions and wafer resistivity, the technique becomes entirely contact resistivity insensitive around 1 mΩcm^2. Indeed, this is consistent with the findings of [82, 93].

Accurate Cox-Strack measurements require that the smallest contact diameter is smaller than twice the wafer thickness: $d_{min} < 2t$ [9]. In the 93 articles studied here, the contact diameters were documented (or obtained from a corresponding author) in 71 papers. Only

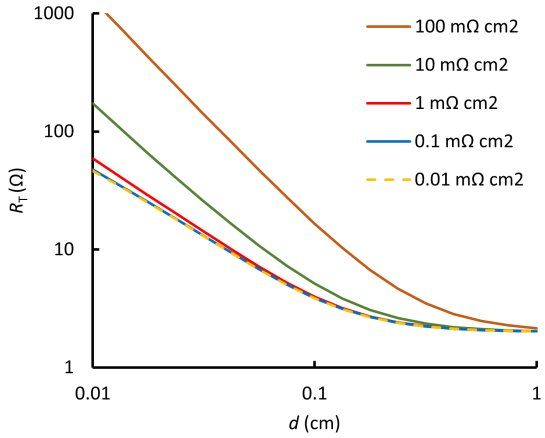

Figure 4: Theoretical curves of total resistance R_T as a function of contact diameter for a wide range of contact resistivities between 0.01 and 100 mΩcm^2. The lower-resistivity curves are indistinguishable as they are dominated by spreading resistance. The curves are produced with equations 1,2,5 using the values ρ_w = 1 Ωcm, R_0 = 2 Ω, and t = 200 μm.

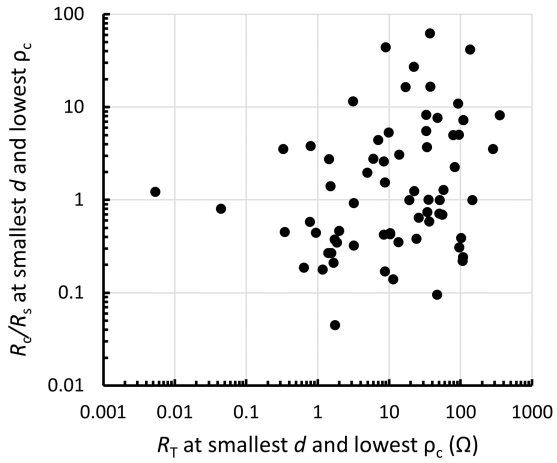

Figure 5: The ratio of contact resistance to spreading resistance for the contact with the smallest diameter and the smallest contact resistivity per paper, as estimated using equations 2 and 5. The ratio is plotted as a function of the total resistance R_T, indicating that low R_c over R_s values appear across a broad range of measured resistance values.

26 of these make use of contacts smaller than twice the wafer thickness, rendering the reported ρ_c values in at least 45 articles questionable.

A different diameter consideration follows from the overall measurement accuracy of R_T. Instrumental effects such as drift, white noise and internal resistance of the ammeter lead to a limited accuracy of any resistance measurement. Typically it is dominated by a relative measurement error. In view of equation 1, it is therefore important that R_c is a significant term in R_T.

For those papers that documented the minimum contact diameter d_{min}, we estimated R_c and R_s of the smallest contact using equations 2 and 5. The result is shown in Figure 5. As the figure indicates, in some cases the lowest contact resistivity has been determined on the basis of a set of measurements that are completely dominated by the spreading resistance. As many as 23 out of 68 papers rely on measurements with $R_c/R_s < 0.5$ (a somewhat arbitrarily set threshold). As a consequence, the reported ρ_c values may have a large statistical error. Not surprisingly, this R_c/R_s criterion identifies the same measurements as 'inaccurate' as the previous two criteria.

To conclude, given the need for low-resistivity contacts in solar cells, there is clear room for improvement in the choice of contact diameters for the Cox-Strack test structure. Contacts much smaller than 1 mm in diameter seem necessary to investigate resistivities in the range of 1 mΩcm^2 (cf. Figure 4). Further, in case contact resistivities below 1 mΩcm^2 are pursued, small contact diameters alone will not suffice. It may then be better to reduce the spreading resistance with thin, higher doped substrates; or to use the Transmission Line Method (TLM) [106] instead.

5.2. *The largest contact*

Large-diameter contacts are less useful for the quantification of low contact resistivities. However, they enable the determination of the substrate resistivity and residual resistance R_0. For these parameters, the choice of contact diameters is less critical. This can be deduced from Figure 6. Again we used dimensions and resistivities typical for contemporary solar cell research as numerical input for the figure (see the figure caption).

The figure shows that the substrate resistivity affects the total resistance for a wide range of diameters. Further, for the given dimensions and contact resistivity, the Cox-Strack method loses sensitivity for wafer resistivities below 1 Ωcm. Such low-ohmic wafers were indeed used in 24% of the analyzed articles. The parameter fitting is in that case best done by a fixed wafer resistivity. In other cases, fitting of the wafer resistivity from the data is advised [9].

Finally, the accuracy of the residual resistance R_0 is, to our opinion, of less concern because it tends to be rather insignificant (especially in the smaller contacts).

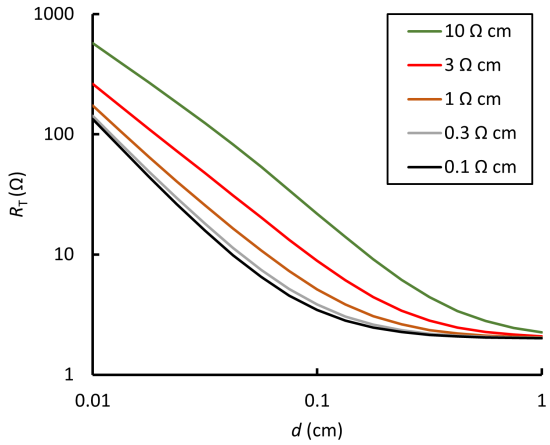

Figure 6: Theoretical curves of total resistance R_T as a function of contact diameter for substrate resistivities between 0.1 and 10 Ωcm. The lower-resistivity curves are hard to distinguish as they are dominated by contact resistance over the full d range. The curves are produced with equations 1,2,5 using the values $\rho_c = 10$ mΩcm^2, $R_0 = 2$ Ω, and $t = 200$ μm.

6. Multilayer top contacts

The Cox-Strack method was devised for a three-layer stack as depicted in Fig. 2. The top contact in this case consists of a single metallic film. Yet, of the studied 93 articles, as many as 77 investigate a top contact composed of more than one layer. In particular, metal - metal oxide - silicon stacks are covered in 52 articles, while 25 articles deal with polysilicon-tunnel oxide contacts to silicon. The resistive top coatings are usually not patterned; only the upper metal is. Figure 7 presents the general layout of such contacts. In this article we refer to such contact schemes as "multilayer top contacts", as the current passes through more than one layer before reaching the semiconductor.

Besides the earlier ρ_w, ρ_c, d and t, three additional parameters come into play: the thickness and the sheet resistance of the conducting coating (t_{film} and $R_\square$ respectively); and a second contact resistivity ρ_c' as indicated in the figure. This second contact resistivity, between resistive coating and substrate, is usually the bottleneck.

In such geometries, two additional accuracy concerns appear with the Cox-Strack method. First, the current may spread in the top film, leading to a larger effective contact diameter between the top film and the substrate. From the analysis in [9] it follows that the current spreads with an effective angle between 45° and 52° in the ideal Cox-Strack configuration, that is, when the two metal contacts have infinite conductivity. The present case is quite different; much wider spreading angles

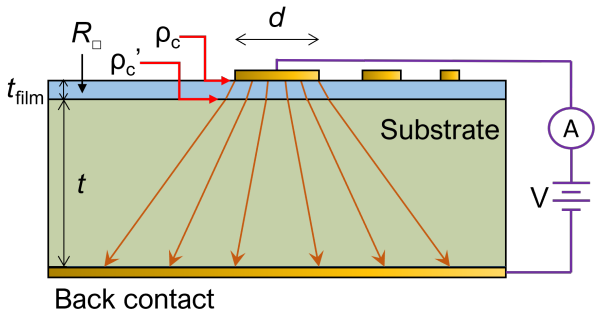

Figure 7: Typical multilayer top contact as investigated in most of the reviewed papers. A thin conducting film (often doped polysilicon or a transition metal oxide) covers the entire substrate. This configuration introduces additional current spreading and additional resistance; see text.

may occur when the thin film has a high conductivity and/or a high contact resistivity ρ_c' towards the substrate [11].

Based on simulations and calculations for a wide range of possible configurations, Turkay *et al.* [11] propose that current spreading in the conductive film can be safely neglected when the following criterion is met:

$$\frac{R_\square d^2}{\rho_c' + \rho_w t + \rho_b} > 900, \tag{7}$$

where ρ_b denotes the contact resistivity between the substrate and the back contact. The equation directly shows that one should be careful when low sheet resistance films are used in combination with small contact diameters. In the following, we neglect ρ_b (which is seldom specified in the reviewed papers).

Of the 77 papers with a multilayer top contact, we were able to obtain $R_\square$, ρ_c', ρ_w, d and t from only 19. Eleven of those fail the test, by a combination of low sheet resistance and small contacts. Studies of polysilicon-tunnel oxide stacks commonly face this problem. Eight articles pass the criterion. Of 50 others with incomplete data, it is safe to assume that the criterion is met because the conductive film is an extremely thin tunnelling layer (a few-nm insulator) and/or highly resistive ($R_\square \gg 1$ kΩ/□), for instance molybdenum oxide.

When highly conducting coatings are used, it is advised to pattern these along with the top metal for the purpose of the Cox-Strack measurement, as several authors indeed do (e.g. [8, 78, 89, 99, 101]). Alternatively, one may resort to multilayer spreading resistance models [11].

A second concern with multilayer top contacts is that the resistance inside the thin film may be significant in

the total measured resistance. Recent works [11],[82] consider such a situation. The total vertical resistance of the conductive film in a contact configuration has an upper limit:

$$R_{\mathrm{film}} \leq \frac{4R_{\square}t_{\mathrm{film}}^2}{\pi d^2}. \tag{8}$$

Equality in the equation above represents the situation where current spreading is negligible.

In the studied papers, $5 \times 10^{-7} \leq t_{\mathrm{film}}/d \leq 2 \times 10^{-4}$. For highly doped polysilicon - tunnel oxide stacks, this makes R_{film} negligible. For metal oxide containing stacks, much higher sheet resistances can be expected. The sheet resistance is hardly ever quoted in the reviewed articles, however. Generally, R_{film} is a negligible amount compared to the contact resistivity only if

$$R_{\square}t_{\mathrm{film}}^2 \ll \rho_{\mathrm{c}}. \tag{9}$$

If not, the contact resistivity is overestimated by the series resistivity in the thin film, which amounts to $R_{\square}{t_{\mathrm{film}}}^2$ at most.

7. Discussion and recommendations

The Cox-Strack method has a limited span for contact resistivity determination. For typical photovoltaic samples, the method gradually becomes insensitive below 10 mΩcm^2, whereas much lower contact resistivities are pursued for high-efficiency cells. The method further systematically overestimates low resistivities, depending on the choice of substrate and the equations used in the analysis. A careful measurement approach can partly mitigate these issues.

Section 5 showed that the choice of contact diameters is critical; the smallest contact being the most important. Technical limitations sometimes lead to the use of oversized contacts. Further, it appears common practice to use the mask-design dimensions in the analysis. Particularly when shadow masks are used, the on-wafer contact dimensions may differ appreciably and the contact area is better measured up by microscope [107].

Table 2 summarizes the effect of these limitations on the accuracy of recently published contact resistivity values. The systematic inaccuracy of the Cox-Strack method at low $\rho_{\mathrm{c}}/\rho_{\mathrm{w}}t$ ratios becomes higher than 10% in 12 of the 93 reviewed papers. As many as 43 articles use too-large contact diameters to accurately separate contact resistivity from spreading resistance. And eleven of the reviewed papers use a multilayer top contact containing a blanket conductive film in which spreading resistance cannot be neglected; including 2 papers that did pass the other tests.

Table 2: Articles tested against the accuracy criteria formulated in Sections 4–6. The lowest "multilayer" criterion is only applied on the 77 articles that treat contact stacks as in Figure 7.

Criterion	Pass	Uncertain	Fail
$\frac{\rho_{\mathrm{c}}}{\rho_{\mathrm{w}}t} > 0.12$	76	5	12
$d_{\mathrm{min}} < 2t$	26	24	43
$R_{\mathrm{c}}/R_{\mathrm{s}} > 0.5$ at d_{min}	45	25	23
All three above	21	20	52
$\frac{R_{\square}d^2}{\rho_{\mathrm{c}}'+\rho_{\mathrm{w}}t+\rho_{\mathrm{b}}} > 900$	57	9	11

Combining these criteria, the lowest reported ρ_{c} values in as many as 54 articles are less accurate than one may expect. The accuracy remains uncertain for 20 papers by lack of information. We can only state with certainty that 19 articles out of 93 report accurate Cox-Strack results, judging by the applied criteria. Contact resistivities in the accurate papers are 10 mΩcm^2 or higher. One is tempted to conclude that the Cox-Stack method is suitable for blanket (continuous backside) contacts, but insufficiently accurate to evaluate grid-style solar cell metallization. However, there is room for improvement in the followed approach.

On the positive side, metal-oxide based multilayer top contacts as developed for photovoltaic cells can be characterized by the Cox-Strack method without additional measures. The computed contact resistivity will then include the oxide's resistance contribution unless it is separately quantified and deducted. For polysilicon-tunnel oxide configurations, the Cox-Strack method is error-prone because of current spreading in the polysilicon.

Given the rising popularity of the Cox-Strack method, it is urgent to formulate guidelines for accurate contact resistivity determination. This is of particular importance as the method loses accuracy at lower contact resistivities and the photovoltaics community should be able to compare experimental results on an equal basis. It is recommended to:

- use a wide range of contact diameters, including one or more that are smaller than twice the wafer thickness;
- avoid the traditional Cox-Strack expression for spreading resistance (equation 3) but use a more accurate formulation such as presented in [6, 9, 11] instead;
- use a substrate that is sufficiently conductive for the contact resistance R_{c} to be significant in the smaller contacts;

- etch off a conductive film in case of multilayer top contacts if possible;
- quantify the series resistivity in case a high-ohmic top layer such as a metal oxide is used between the substrate and the metal contact, and correct ρ_c for it;
- use measured values for the contact areas instead of mask dimensions;
- specify the wafer resistivity, its thickness and the diameters of the circular contacts in publications.

In the studied articles, an error estimate for the calculated contact resistivity is hardly ever provided. For contact resistivities around or below 10 mΩcm^2 we recommend that the presented findings should be accompanied by an error analysis that goes beyond a statistical or fitting error (see e.g. [8, 11]).

The TLM method is a higher-accuracy alternative to Cox-Strack for such low contact resistivities [108, 109]. In 2021, as many as 60 photovoltaics-related publications were found in the Scopus database that use TLM for contact resistivity determination. It should however be mentioned that the lateral conductivity in multilayer top contacts is much more problematic for TLM measurements than in the Cox-Strack method. Error estimation is also recommended for low-ρ_c quantification with this method.

Conclusion

Recent reports of contact resistance as measured using the Cox-Strack method are reviewed for their accuracy in this work. Almost half of the 93 articles uses too large contact diameters, which makes the method insensitive to contact resistivity and the result noisy. Further, a higher than 10% systematic overestimate of contact resistivity is found in 12 of the 93 papers. Another 11 articles suffer from spreading resistance in a conductive top layer. Consequently, the lowest contact resistivities reported in at least 54 of the articles are inaccurate, which makes the comparison between published results from different papers difficult. Recommendations are given for improved-accuracy Cox-Strack measurements and their analysis.

Acknowledgments

The authors would like to thank the 28 corresponding authors who kindly supplied additional information about their published work.

References

[1] M. Leilaeioun, W. Weigand, M. Boccard, Z. Yu, K. Fisher, Z. Holman, Contact resistivity of the p-type amorphous silicon hole contact in silicon heterojunction solar cells, IEEE Journal of Photovoltaics 10 (1) (2020) 54–62.

[2] R. Brendel, R. Peibst, Contact selectivity and efficiency in crystalline silicon photovoltaics, IEEE Journal of Photovoltaics 6 (6) (2016) 1413–1420.

[3] D. Schroder, D. Meier, Solar cell contact resistance—a review, IEEE Transactions on Electron Devices 31 (5) (1984) 637–647.

[4] R. Cox, H. Strack, Ohmic contacts for GaAs devices, Solid State Electronics 10 (12) (1967) 1213–1214,IN7–IN8,1215–1218.

[5] Retrieved from www.scopus.com as all documents citing [4], January 2022.

[6] M. Denhoff, An accurate calculation of spreading resistance, Journal of Physics D: Applied Physics 39 (9) (2006) 1761–1765.

[7] S. Kristiansson, F. Ingvarson, K. Jeppson, Compact spreading resistance model for rectangular contacts on uniform and epitaxial substrates, IEEE Transactions on Electron Devices 54 (9) (2007) 2531–2536.

[8] K. Fong, T. Kho, W. Liang, T. Chong, M. Ernst, D. Walter, M. Stocks, E. Franklin, K. McIntosh, A. Blakers, Optimization and characterization of phosphorus diffused LPCVD polysilicon passivated contacts with low pressure tunnel oxide, in: 2018 IEEE 7th World Conference on Photovoltaic Energy Conversion, WCPEC 2018 - A Joint Conference of 45th IEEE PVSC, 28th PVSEC and 34th EU PVSEC, 2018, pp. 2002–2005.

[9] M. Van Rijnbach, R. Hueting, M. Stodolny, G. Janssen, J. Melskens, J. Schmitz, On the accuracy of the Cox-Strack equation and method for contact resistivity determination, IEEE Transactions on Electron Devices 67 (4) (2020) 1757–1763.

[10] B. Gelmont, M. Shur, Spreading resistance of a round ohmic contact, Solid State Electronics 36 (2) (1993) 143–146.

[11] D. Turkay, K. Tsoi, E. Donercark, R. Turan, S. Yerci, Spreading resistance modeling for contact resistivity extraction in ohmic multilayer structures with circular electrodes, IEEE Transactions on Electron Devices 68 (12) (2021) 6344–6351.

[12] S. Cheung, N. Cheung, Extraction of Schottky diode parameters from forward current-voltage characteristics, Applied Physics Letters 49 (2) (1986) 85–87.

[13] S. Kailasam, R. Vijayan, D. Amirthaganesan, S. Srinath, V. Viswanathan, S. Masilamani, P. Krishnamoorthy, M. Varadharajaperumal, Accuracy of contact resistivity measurements for electron-selective titanium oxide contacts in n-type c-Si solar cell, IEEE Journal of Photovoltaics 11 (3) (2021) 613–619.

[14] J. Tong, Y. Wan, J. Cui, S. Lim, N. Song, A. Lennon, Solution-processed molybdenum oxide for hole-selective contacts on crystalline silicon solar cells, Applied Surface Science 423 (2017) 139–146.

[15] X. Yang, K. Weber, Z. Hameiri, S. De Wolf, Industrially feasible, dopant-free, carrier-selective contacts for high-efficiency silicon solar cells, Progress in Photovoltaics: Research and Applications 25 (11) (2017) 896–904.

[16] T. Allen, J. Bullock, P. Zheng, B. Vaughan, M. Barr, Y. Wan, C. Samundsett, D. Walter, A. Javey, A. Cuevas, Calcium contacts to n-type crystalline silicon solar cells, Progress in Photovoltaics: Research and Applications 25 (7) (2017) 636–644.

[17] Y. Wan, C. Samundsett, J. Bullock, M. Hettick, T. Allen, D. Yan, J. Peng, Y. Wu, J. Cui, A. Javey, A. Cuevas, Conductive and stable magnesium oxide electron-selective contacts for

efficient silicon solar cells, Advanced Energy Materials 7 (5) (2017).

[18] V. Titova, B. Veith-Wolf, D. Startsev, J. Schmidt, Effective passivation of crystalline silicon surfaces by ultrathin atomic-layer-deposited TiO_x layers, in: Energy Procedia, Vol. 124, 2017, pp. 441–447.

[19] S. Mondal, A. Soman, A. Antony, Optimization and fabrication of rear surface passivated c-Si solar cells on 156 cm^2 area with local point contacts made by microsecond-pulsed laser firing, Solar Energy 158 (2017) 360–366.

[20] T. Zhang, M. Hossain, C.-Y. Lee, Y. Zakaria, A. Abdallah, B. Hoex, Atomic layer deposited $Zn_xNi_{1-x}O$: A thermally stable hole selective contact for silicon solar cells, Applied Physics Letters 113 (26) (2018).

[21] H. Shen, S. Omelchenko, D. Jacobs, S. Yalamanchili, Y. Wan, D. Yan, P. Phang, T. Duong, Y. Wu, Y. Yin, C. Samundsett, J. Peng, N. Wu, T. White, G. Andersson, N. Lewis, K. Catchpole, In situ recombination junction between p-Si and TiO_2 enables high-efficiency monolithic perovskite/Si tandem cells, Science Advances 4 (12) (2018).

[22] Z. Zhang, M. Liao, H. Tong, D. Wang, C. Quan, P. Gao, J. Sheng, W. Guo, J. Yang, Y. Zhang, X. Gong, X. Zhang, B. Yan, X. Zhou, Y. Zeng, J. Ye, Tunnel oxide – magnesium as electron-selective passivated contact for n-type silicon solar cell, Solar RRL 2 (12) (2018).

[23] Z. Wang, Y. Yang, L. Zhang, H. Lin, Z. Zhang, D. Wang, S. Peng, D. He, J. Ye, P. Gao, Modulation-doped ZnO as high performance electron-selective layer for efficient silicon heterojunction solar cells, Nano Energy 54 (2018) 99–105.

[24] Z. Zhang, Y. Zeng, C.-S. Jiang, Y. Huang, M. Liao, H. Tong, M. Al-Jassim, P. Gao, C. Shou, X. Zhou, B. Yan, J. Ye, Carrier transport through the ultrathin silicon-oxide layer in tunnel oxide passivated contact (TOPCon) c-Si solar cells, Solar Energy Materials and Solar Cells 187 (2018) 113–122.

[25] Z. Zou, W. Liu, D. Wang, Z. Liu, E. Jiang, S. Wu, J. Zhu, W. Guo, J. Sheng, J. Ye, Electron-selective quinhydrone passivated back contact for high-efficiency silicon/organic heterojunction solar cells, Solar Energy Materials and Solar Cells 185 (2018) 218–225.

[26] B. Macco, L. Black, J. Melskens, B. van de Loo, W.-J. Berghuis, M. Verheijen, W. Kessels, Atomic-layer deposited Nb_2O_5 as transparent passivating electron contact for c-Si solar cells, Solar Energy Materials and Solar Cells 184 (2018) 98–104.

[27] J. He, Y. Wan, P. Gao, J. Tang, J. Ye, Over 16.7% efficiency organic-silicon heterojunction solar cells with solution-processed dopant-free contacts for both polarities, Advanced Functional Materials 28 (34) (2018).

[28] T. Zhang, C.-Y. Lee, Y. Wan, S. Lim, B. Hoex, Investigation of the thermal stability of MoO_x as hole-selective contacts for Si solar cells, Journal of Applied Physics 124 (7) (2018).

[29] D. Yan, A. Cuevas, S. Phang, Y. Wan, D. Macdonald, 23% efficient p-type crystalline silicon solar cells with hole-selective passivating contacts based on physical vapor deposition of doped silicon films, Applied Physics Letters 113 (6) (2018).

[30] Y. Wan, J. Bullock, M. Hettick, Z. Xu, C. Samundsett, D. Yan, J. Peng, J. Ye, A. Javey, A. Cuevas, Temperature and humidity stable alkali/alkaline-earth metal carbonates as electron heterocontacts for silicon photovoltaics, Advanced Energy Materials 8 (22) (2018).

[31] C. Quan, H. Tong, Z. Yang, X. Ke, M. Liao, P. Gao, D. Wang, Z. Yuan, K. Chen, J. Yang, X. Zhang, C. Shou, B. Yan, Y. Zeng, J. Ye, Electron-selective scandium-tunnel oxide passivated contact for n-type silicon solar cells, Solar RRL 2 (8) (2018).

[32] X. Yang, E. Aydin, H. Xu, J. Kang, M. Hedhili, W. Liu, Y. Wan, J. Peng, C. Samundsett, A. Cuevas, S. De Wolf, Tantalum nitride electron-selective contact for crystalline silicon solar cells, Advanced Energy Materials 8 (20) (2018).

[33] G. Lopez, C. Jin, I. Martin, R. Alcubilla, Impact of c-Si surface passivating layer thickness on n^+ laser-doped contacts based on silicon carbide films, IEEE Journal of Photovoltaics 8 (4) (2018) 976–981.

[34] H. Tong, Z. Yang, X. Wang, Z. Liu, Z. Chen, X. Ke, M. Sui, J. Tang, T. Yu, Z. Ge, Y. Zeng, P. Gao, J. Ye, Dual functional electron-selective contacts based on silicon oxide/magnesium: Tailoring heterointerface band structures while maintaining surface passivation, Advanced Energy Materials 8 (16) (2018).

[35] Z. Yang, P. Gao, J. Sheng, H. Tong, C. Quan, X. Yang, K. Chee, B. Yan, Y. Zeng, J. Ye, Principles of dopant-free electron-selective contacts based on tunnel oxide/low work-function metal stacks and their applications in heterojunction solar cells, Nano Energy 46 (2018) 133–140.

[36] P. Liu, P. Gao, X. Liu, H. Wang, J. He, X. Yang, Y. Zeng, B. Yan, J. Fang, J. Ye, High-performance organic-silicon heterojunction solar cells by using Al-doped ZnO as cathode interlayer, Solar RRL 2 (3) (2018).

[37] Y. Wan, S. Karuturi, C. Samundsett, J. Bullock, M. Hettick, D. Yan, J. Peng, P. Narangari, S. Mokkapati, H. Tan, C. Jagadish, A. Javey, A. Cuevas, Tantalum oxide electron-selective heterocontacts for silicon photovoltaics and photoelectrochemical water reduction, ACS Energy Letters 3 (1) (2018) 125–131.

[38] J. Yu, Y. Fu, L. Zhu, Z. Yang, X. Yang, L. Ding, Y. Zeng, B. Yan, J. Tang, P. Gao, J. Ye, Heterojunction solar cells with asymmetrically carrier-selective contact structure of molybdenum-oxide/silicon/magnesium-oxide, Solar Energy 159 (2018) 704–709.

[39] J. He, W. Zhang, J. Ye, P. Gao, 16% efficient silicon/organic heterojunction solar cells using narrow band-gap conjugated polyelectrolytes based low resistance electron-selective contacts, Nano Energy 43 (2018) 117–123.

[40] T. Truong, D. Yan, C. Samundsett, A. Liu, S. Harvey, M. Young, Z. Ding, M. Tebyetekerwa, F. Kremer, M. Al-Jassim, A. Cuevas, D. MacDonald, H. Nguyen, Hydrogen-assisted defect engineering of doped poly-Si films for passivating contact solar cells, ACS Applied Energy Materials 2 (12) (2019) 8783–8791.

[41] J. Wang, H. Lin, Z. Wang, W. Shen, J. Ye, P. Gao, Hard mask processing of 20% efficiency back-contacted silicon solar cells with dopant-free heterojunctions, Nano Energy 66 (2019) 104116.

[42] K. Gotoh, T. Mochizuki, Y. Kurokawa, N. Usami, Tuning the electrical properties of titanium oxide bilayers prepared by atomic layer deposition at different temperatures, Physica Status Solidi (A) Applications and Materials Science 216 (22) (2019).

[43] L. Jin, L. Cai, D. Chen, W. Wang, H. Shen, F. Zhang, Efficient silicon solar cells applying cuprous sulfide as hole-selective contact, Journal of Materials Science 54 (19) (2019) 12650–12658.

[44] M. Liu, Y. Zhou, G. Dong, W. Wang, J. Wang, C. Liu, F. Liu, D. Yu, SnO_2/Mg combination electron selective transport layer for Si heterojunction solar cells, Solar Energy Materials and Solar Cells 200 (2019).

[45] T. Gao, Q. Yang, X. Guo, Y. Huang, Z. Zhang, Z. Wang, M. Liao, C. Shou, Y. Zeng, B. Yan, G. Hou, X. Zhang, Y. Zhao, J. Ye, An industrially viable TOPCon structure with both ultrathin SiO_x and n+-poly-Si processed by PECVD for p-type c-Si solar cells, Solar Energy Materials and Solar Cells 200 (2019)

109926.

[46] E.-C. Wang, A. Morales-Vilches, S. Neubert, A. Cruz, R. Schlatmann, B. Stannowski, A simple method with analytical model to extract heterojunction solar cell series resistance components and to extract the a-Si:H(I/P) to transparent conductive oxide contact resistivity, in: AIP Conference Proceedings, Vol. 2147, 2019.

[47] J. Yu, M. Liao, D. Yan, Y. Wan, H. Lin, Z. Wang, P. Gao, Y. Zeng, B. Yan, J. Ye, Activating and optimizing evaporation-processed magnesium oxide passivating contact for silicon solar cells, Nano Energy 62 (2019) 181–188.

[48] W. Liu, X. Yang, J. Kang, S. Li, L. Xu, S. Zhang, H. Xu, J. Peng, F. Xie, J.-H. Fu, K. Wang, J. Liu, A. Alzahrani, S. De Wolf, Polysilicon passivating contacts for silicon solar cells: Interface passivation and carrier transport mechanism, ACS Applied Energy Materials 2 (7) (2019) 4609–4617.

[49] W. Wang, H. Lin, Z. Yang, Z. Wang, J. Wang, L. Zhang, M. Liao, Y. Zeng, P. Gao, B. Yan, J. Ye, An expanded Cox and Strack method for precise extraction of specific contact resistance of transition metal oxide/n-silicon heterojunction, IEEE Journal of Photovoltaics 9 (4) (2019) 1113–1120.

[50] J. He, M. Hossain, H. Lin, W. Wang, S. Karuturi, B. Hoex, J. Ye, P. Gao, J. Bullock, Y. Wan, 15% efficiency ultrathin silicon solar cells with fluorine-doped titanium oxide and chemically tailored poly(3,4-ethylenedioxythiophene):poly(styrenesulfonate) as asymmetric heterocontact, ACS Nano 13 (6) (2019) 6356–6362.

[51] T. Zhang, M. Hossain, K. Thong Khoo, C.-Y. Lee, Y. Zakaria, A. Abdallah, B. Hoex, Atomic layer deposited Al_xNi_yO as hole selective contact for silicon solar cells, in: Conference Record of the IEEE Photovoltaic Specialists Conference, 2019, pp. 2338–2341.

[52] X. Yang, W. Liu, M. De Bastiani, T. Allen, J. Kang, H. Xu, E. Aydin, L. Xu, Q. Bi, H. Dang, E. AlHabshi, K. Kotsovos, A. AlSaggaf, I. Gereige, Y. Wan, J. Peng, C. Samundsett, A. Cuevas, S. De Wolf, Dual-function electron-conductive, hole-blocking titanium nitride contacts for efficient silicon solar cells, Joule 3 (5) (2019) 1314–1327.

[53] D. Yan, S. Phang, Y. Wan, C. Samundsett, D. Macdonald, A. Cuevas, High efficiency n-type silicon solar cells with passivating contacts based on PECVD silicon films doped by phosphorus diffusion, Solar Energy Materials and Solar Cells 193 (2019) 80–84.

[54] T. Mochizuki, K. Gotoh, Y. Kurokawa, T. Yamamoto, N. Usami, Local structure of high performance tio x electron-selective contact revealed by electron energy loss spectroscopy, Advanced Materials Interfaces 6 (3) (2019).

[55] E. Khorani, S. McNab, T. Scheul, T. Rahman, R. Bonilla, S. Boden, P. Wilshaw, Optoelectronic properties of ultra-thin ALD silicon nitride and its potential as a hole-selective nanolayer for high efficiency solar cells, APL Materials 8 (11) (2020).

[56] A. Alzahrani, T. Allen, M. De Bastiani, E. Van Kerschaver, G. Harrison, W. Liu, S. De Wolf, In situ plasma-grown silicon-oxide for polysilicon passivating contacts, Advanced Materials Interfaces 7 (21) (2020).

[57] Z. Lu, X. Liu, G. Hou, J. Chen, T. Zhu, J. Xu, K. Chen, Doping-free titanium nitride carrier selective contacts for efficient organic-inorganic hybrid solar cells, ACS Applied Energy Materials 3 (9) (2020) 9208–9215.

[58] D. Hiller, P. Hönicke, D. König, Material combination of tunnel-SiO_2 with a (sub-)monolayer of ALD-AlO_x on silicon offering a highly passivating hole selective contact, Solar Energy Materials and Solar Cells 215 (2020).

[59] T. Truong, D. Yan, W. Chen, W. Wang, H. Guthrey, M. Al-Jassim, A. Cuevas, D. Macdonald, H. Nguyen, Deposition pressure dependent structural and optoelectronic properties of ex-situ boron-doped poly-Si/SiO_x passivating contacts based on sputtered silicon, Solar Energy Materials and Solar Cells 215 (2020).

[60] W. Chen, J. Stuckelberger, W. Wang, S. Phang, D. Kang, C. Samundsett, D. MacDonald, A. Cuevas, L. Zhou, Y. Wan, D. Yan, Influence of PECVD deposition power and pressure on phosphorus-doped polysilicon passivating contacts, IEEE Journal of Photovoltaics 10 (5) (2020) 1239–1245.

[61] X. Yang, H. Xu, W. Liu, Q. Bi, L. Xu, J. Kang, M. Hedhili, B. Sun, X. Zhang, S. De Wolf, Atomic layer deposition of vanadium oxide as hole-selective contact for crystalline silicon solar cells, Advanced Electronic Materials 6 (8) (2020).

[62] X. Yang, Y. Lin, J. Liu, W. Liu, Q. Bi, X. Song, J. Kang, F. Xu, L. Xu, M. Hedhili, D. Baran, X. Zhang, T. Anthopoulos, S. De Wolf, A highly conductive titanium oxynitride electron-selective contact for efficient photovoltaic devices, Advanced Materials 32 (32) (2020).

[63] N. Mozaffari, H. Shen, Y. Yin, Y. Li, D. Hiller, D. Jacobs, H. Nguyen, P. Phang, G. Andersson, U. Kaiser, T. White, K. Weber, K. Catchpole, Efficient passivation and low resistivity for p^+-Si/TiO_2 contact by atomic layer deposition, ACS Applied Energy Materials 3 (7) (2020) 6291–6301.

[64] D. Hiller, J. Julin, A. Chnani, S. Strehle, Silicon surface passivation by ALD-Ga_2O_3: Thermal vs. plasma-enhanced atomic layer deposition, IEEE Journal of Photovoltaics 10 (4) (2020) 959–968.

[65] J. Kang, W. Liu, T. Allen, M. De Bastiani, X. Yang, S. De Wolf, Intrinsic silicon buffer layer improves hole-collecting poly-Si passivating contact, Advanced Materials Interfaces 7 (13) (2020).

[66] X. Guo, M. Liao, Z. Rui, Q. Yang, Z. Wang, C. Shou, W. Ding, X. Luo, Y. Cao, J. Xu, L. Fu, Y. Zeng, B. Yan, J. Ye, Comparison of different types of interfacial oxides on hole-selective p^+-poly-Si passivated contacts for high-efficiency c-Si solar cells, Solar Energy Materials and Solar Cells 210 (2020).

[67] B. Davis, N. Strandwitz, A systematic investigation of aluminum oxide passivating tunnel layers for titanium oxide electron-selective contacts, in: Conference Record of the IEEE Photovoltaic Specialists Conference, Vol. 2020-June, 2020, pp. 1557–1561.

[68] A. Le, R. Basnet, D. Yan, W. Chen, J. Seif, Z. Hameiri, Temperature dependence of polysilicon passivating contact and its device performance, in: Conference Record of the IEEE Photovoltaic Specialists Conference, Vol. 2020-June, 2020, pp. 1020–1023.

[69] J. Yu, J. Yu, J. Yu, P. Phang, C. Samundsett, R. Basnet, G. Neupan, X. Yang, D. Macdonald, Y. Wan, D. Yan, J. Ye, Titanium nitride electron-conductive contact for silicon solar cells by radio frequency sputtering from a TiN target, ACS Applied Materials and Interfaces 12 (23) (2020) 26177–26183.

[70] B. Davis, N. Strandwitz, Aluminum oxide passivating tunneling interlayers for molybdenum oxide hole-selective contacts, IEEE Journal of Photovoltaics 10 (3) (2020) 722–728.

[71] L. Wan, C. Zhang, K. Ge, X. Yang, F. Li, W. Yan, Z. Xu, L. Yang, Y. Xu, D. Song, J. Chen, Conductive hole-selective passivating contacts for crystalline silicon solar cells, Advanced Energy Materials 10 (16) (2020).

[72] G. Chistiakova, B. Macco, L. Korte, Low-temperature atomic layer deposited magnesium oxide as a passivating electron contact for c-Si-based solar cells, IEEE Journal of Photovoltaics 10 (2) (2020) 398–406.

[73] W. Wang, J. He, D. Yan, C. Samundsett, S. Phang, Z. Huang, W. Shen, J. Bullock, Y. Wan, 21.3%-efficient n-type silicon

solar cell with a full area rear TiO_x/LiF/Al electron-selective contact, Solar Energy Materials and Solar Cells 206 (2020).

[74] W. Chen, T. Truong, H. Nguyen, C. Samundsett, S. Phang, D. MacDonald, A. Cuevas, L. Zhou, Y. Wan, D. Yan, Influence of PECVD deposition temperature on phosphorus doped poly-silicon passivating contacts, Solar Energy Materials and Solar Cells 206 (2020).

[75] Y. Lin, Z. Yang, Z. Liu, J. Zheng, M. Feng, Y. Zhi, L. Lu, M. Liao, W. Liu, D. Ma, Q. Han, H. Cheng, Q. Zeng, Z. Yuan, B. Yan, Y. Zeng, J. Ye, Dual-functional carbon-doped polysilicon films for passivating contact solar cells: Regulating physical contacts while promoting photoelectrical properties, Energy and Environmental Science 14 (12) (2021) 6406–6418.

[76] T. Truong, T. Le, D. Yan, S. Phang, M. Tebyetekerwa, M. Young, M. Al-Jassim, A. Cuevas, D. Macdonald, J. Stuckelberger, H. Nguyen, Investigation of gallium–boron spin-on codoping for poly-Si/SiO_x passivating contacts, Solar RRL 5 (12) (2021).

[77] C. Shou, J. Zheng, Q. Han, Y. Zeng, W. Ding, H. He, M. Liao, X. Yang, J. Sheng, B. Yan, J. Ye, Optimization of tunnel-junction for perovskite/tunnel oxide passivated contact (TOPCon) tandem solar cells, Physica Status Solidi (A) Applications and Materials Science 218 (24) (2021).

[78] Y. Li, Y. Li, G. Zhang, J. Li, D. Liang, Y. Wu, T. Song, X. Yang, D. Li, C. Jiang, B. Sun, Stable molybdenum nitride contact for efficient silicon solar cells, Physica Status Solidi - Rapid Research Letters 15 (12) (2021).

[79] G. Du, L. Li, X. Yang, X. Zhou, Z. Su, P. Cheng, Y. Lin, L. Lu, J. Wang, L. Yang, X. Gao, X. Chen, D. Li, Improved V_2O_x passivating contact for p-type crystalline silicon solar cells by oxygen vacancy modulation with a SiO_x tunnel layer, Advanced Materials Interfaces 8 (22) (2021).

[80] W. Chen, J. Stuckelberger, W. Wang, S. Phang, D. Macdonald, Y. Wan, D. Yan, N-type polysilicon passivating contacts using ultra-thin PECVD silicon oxynitrides as the interfacial layer, Solar Energy Materials and Solar Cells 232 (2021).

[81] Y. Nakagawa, K. Gotoh, T. Inoue, Y. Kurokawa, N. Usami, Improved performance of titanium oxide/silicon oxide electron-selective contacts by implementation of magnesium interlayers, Physica Status Solidi (A) Applications and Materials Science 218 (19) (2021).

[82] N. Folchert, R. Brendel, Extended Cox & Strack analysis for the contact resistance of planar samples with carrier-selective junctions on both sides, Solar Energy Materials and Solar Cells 231 (2021).

[83] S. Miyagawa, K. Gotoh, K. Kutsukake, Y. Kurokawa, N. Usami, Application of Bayesian optimization for high-performance TiO_x/SiO_y/c-Si passivating contact, Solar Energy Materials and Solar Cells 230 (2021).

[84] V. Titova, J. Schmidt, Selectivity of TiO_x-based electron-selective contacts on n-type crystalline silicon and solar cell efficiency potential, Physica Status Solidi - Rapid Research Letters 15 (9) (2021).

[85] J. Chen, C. Liu, S. Xu, P. Wang, X. Ge, B. Han, Y. Zhang, M. Wang, X. Wu, L. Xu, P. Lin, X. Huang, X. Yu, C. Cui, Solution-processed molybdenum oxide films by low-temperature annealing for improved silicon surface passivation, Materials Science in Semiconductor Processing 132 (2021).

[86] J. Tong, T. Le, W. Liang, M. Hossain, K. McIntosh, P. Narangari, S. Armand, T. Kho, K. Khoo, Y. Zakaria, A. Abdallah, S. Surve, M. Ernst, B. Hoex, K. Fong, Impact of pre-grown SiO_x on the carrier selectivity and thermal stability of molybdenum-oxide-passivated contact for Si solar cells, ACS Applied Materials and Interfaces 13 (30) (2021) 36426–36435.

[87] B. Garland, B. Davis, N. Strandwitz, Exploiting fixed charge to control Schottky barrier height in Si—Al_2O_3—MoO_x- based tunnel diodes, in: Conference Record of the IEEE Photovoltaic Specialists Conference, 2021, pp. 2439–2442.

[88] R. Tsubata, K. Gotoh, M. Matsumi, M. Wilde, T. Inoue, Y. Kurokawa, K. Fukutani, N. Usami, Silicon nanocrystals embedded in nanolayered silicon oxide for crystalline silicon solar cells, ACS Applied Nano Materials (2021).

[89] A. Tuan Le, R. Basnet, D. Yan, W. Chen, N. Nandakumar, S. Duttagupta, J. Seif, Z. Hameiri, Temperature-dependent performance of silicon solar cells with polysilicon passivating contacts, Solar Energy Materials and Solar Cells 225 (2021).

[90] J. Qiu, X. Lv, Q. Ren, Y. Yang, Y. Mai, Dual bilayer for improving contact quality and passivation enables efficient organic/planar-Si hybrid solar cells with a champion V_{OC} of over 656 mV, ACS Applied Energy Materials 4 (5) (2021) 5000–5006.

[91] Z. Wang, J. He, W. Wang, H. Lin, Z. Xu, Q. Liu, S. Peng, J. Hou, D. He, P. Gao, Twenty percent efficiency crystalline silicon solar cells with solution-processed electron-selective contacts, ACS Applied Energy Materials 4 (4) (2021) 3644–3650.

[92] X. Yang, Z. Ying, Z. Yang, J.-R. Xu, W. Wang, J. Wang, Z. Wang, L. Yao, B. Yan, J. Ye, Light-promoted electrostatic adsorption of high-density lewis base monolayers as passivating electron-selective contacts, Advanced Science 8 (5) (2021).

[93] Z. Ding, D. Yan, J. Stuckelberger, S. Phang, W. Chen, C. Samundsett, J. Yang, Z. Wang, P. Zheng, X. Zhang, Y. Wan, D. Macdonald, Phosphorus-doped polycrystalline silicon passivating contacts via spin-on doping, Solar Energy Materials and Solar Cells 221 (2021).

[94] H. Nasser, F. Es, M. Zolfaghari Borra, E. Semiz, G. Kökbudak, E. Orhan, R. Turan, On the application of hole-selective MoO_x as full-area rear contact for industrial scale p-type c-Si solar cells, Progress in Photovoltaics: Research and Applications 29 (3) (2021) 281–293.

[95] X. Yang, J. Kang, W. Liu, X. Zhang, S. de Wolf, Solution-doped polysilicon passivating contacts for silicon solar cells, ACS Applied Materials and Interfaces 13 (7) (2021) 8455–8460.

[96] Z. Lu, G. Hou, Y. Zhu, J. Chen, J. Xu, K. Chen, High efficiency organic-Si hybrid solar cells with a one-dimensional CdS interlayer, Nanoscale 13 (7) (2021) 4206–4212.

[97] L. Yao, Z. Ying, W. Wang, Z. Yang, J. Sun, X. Wang, X. Yang, Y. Zeng, B. Yan, X. Xu, J. Ye, Solution-processed and annealing-free zirconium acetylacetonate electron-selective contacts for efficient crystalline silicon solar cells, Solar Energy 215 (2021) 410–415.

[98] T. Pan, J. Li, Y. Lin, Z. Xue, Z. Di, M. Yin, J. Wang, L. Lu, L. Yang, D. Li, Structural and optical studies of molybdenum oxides thin films obtained by thermal evaporation and atomic layer deposition methods for photovoltaic application, Journal of Materials Science: Materials in Electronics 32 (3) (2021) 3475–3486.

[99] L. Chen, H. Lin, Z. Liu, T. Wu, Y. Pang, P. Gao, W. Shen, Realization of a general method for extracting specific contact resistance of silicon-based dopant-free heterojunctions, Solar RRL (2021).

[100] A. Le, J. Dréon, J. Michel, M. Boccard, J. Bullock, N. Borojevic, Z. Hameiri, Temperature-dependent performance of silicon heterojunction solar cells with transition-metal-oxide-based selective contacts, Progress in Photovoltaics: Research and Applications (2021).

[101] H. Nasser, M. Borra, E. Çiftpınar, B. Eldeeb, R. Turan, Fourteen percent efficiency ultrathin silicon solar cells with improved infrared light management enabled by hole-selective

transition metal oxide full-area rear passivating contacts, Progress in Photovoltaics: Research and Applications (2021).
[102] J. Kang, X. Yang, W. Liu, J. Liu, H. Xu, T. Allen, S. De Wolf, Electron-selective lithium contacts for crystalline silicon solar cells, Advanced Materials Interfaces (2021).
[103] Y. Jiang, S. Cao, L. Lu, G. Du, Y. Lin, J. Wang, L. Yang, W. Zhu, D. Li, Post-annealing effect on optical and electronic properties of thermally evaporated MoO_x thin films as hole-selective contacts for p-Si solar cells, Nanoscale Research Letters 16 (1) (2021).
[104] K. Gotoh, T. Mochizuki, T. Hojo, Y. Shibayama, Y. Kurokawa, E. Akiyama, N. Usami, Activation energy of hydrogen desorption from high-performance titanium oxide carrier-selective contacts with silicon oxide interlayers, Current Applied Physics 21 (2021) 36–42.
[105] Quintessa, GraphGrabber version 2.0.2, downloaded from www.quintessa.org/graph-grabber.
[106] D. Schroder, Semiconductor Material and Device Characterization: Third Edition, 2005.
[107] B. Davis, Lehigh University, personal communication.
[108] H.-J. Ueng, D. Janes, K. Webb, Error analysis leading to design criteria for transmission line model characterization of ohmic contacts, IEEE Transactions on Electron Devices 48 (4) (2001) 758–766.
[109] M. Rienacker, M. Bossmeyer, A. Merkle, U. Romer, F. Haase, J. Krugener, R. Brendel, R. Peibst, Junction resistivity of carrier-selective polysilicon on oxide junctions and its impact on solar cell performance, IEEE Journal of Photovoltaics 7 (1) (2017) 11–18.